Check for updates

Received: 13 February 2022 | Revised: 26 October 2022 | Accepted: 25 November 2022

DOI: 10.1002/hbm.26173

RESEARCH ARTICLE

WILEY

Coordinated anatomical and functional variability in the human brain during adolescence

John Bero[1] | Yang Li[1] | Aviral Kumar[1] | Colin Humphries[1] | Snehesh Nag[1] | Heungyeol Lee[1] | Woo Young Ahn[2] | Sowon Hahn[2] | Robert Todd Constable[3] | Hackjin Kim[4] | Daeyeol Lee[1,5,6,7,8]

[1]Neurogazer, Inc., Baltimore, Maryland, USA

[2]Department of Psychology, Seoul National University, Seoul, Korea

[3]Department of Diagnostic Radiology and Neurosurgery, Yale School of Medicine, New Haven, Connecticut, USA

[4]Department of Psychology, Korea University, Seoul, Korea

[5]The Zanvyl Krieger Mind/Brain Institute, Johns Hopkins University, Baltimore, Maryland, USA

[6]Department of Neuroscience, Johns Hopkins University, Baltimore, Maryland, USA

[7]Department of Psychological and Brain Sciences, Johns Hopkins University, Baltimore, Maryland, USA

[8]Kavli Neuroscience Discovery Institute, Johns Hopkins University, Baltimore, Maryland, USA

Correspondence
Daeyeol Lee, The Zanvyl Krieger Mind/Brain Institute, Johns Hopkins University, 3400 North Charles St., 338 Krieger Hall, Baltimore, MD 21218, USA.
Email: daeyeol@jhu.edu

Funding information
Neurogazer, Inc.

Abstract

Adolescence represents a time of unparalleled brain development. In particular, developmental changes in morphometric and cytoarchitectural features are accompanied by maturation in the functional connectivity (FC). Here, we examined how three facets of the brain, including myelination, cortical thickness (CT), and resting-state FC, interact in children between the ages of 10 and 15. We investigated the pattern of coordination in these measures by computing correlation matrices for each measure as well as meta-correlations among them both at the regional and network levels. The results revealed consistently higher meta-correlations among myelin, CT, and FC in the sensory-motor cortical areas than in the association cortical areas. We also found that these meta-correlations were stable and little affected by age-related changes in each measure. In addition, regional variations in the meta-correlations were consistent with the previously identified gradient in the FC and therefore reflected the hierarchy of cortical information processing, and this relationship persists in the adult brain. These results demonstrate that heterogeneity in FC among multiple cortical areas are closely coordinated with the development of cortical myelination and thickness during adolescence.

KEYWORDS
covariance, functional, MRI, resting-state networks, structural

1 | INTRODUCTION

Childhood and adolescence are times of active morphological and functional maturation in the brain with important implications for cognitive developments and psychological states. The morphological transformation during these early years is characterized by the thinning of the cortical gray matter as well as increased synaptic pruning and myelination underneath the cortex (Grydeland et al., 2013; Huttenlocher, 1979; Natu et al., 2019; Selemon, 2013; Tau & Peterson, 2010). These structural-developmental processes are thought to facilitate information flow across cortical regions and reconfigure brain connectivity into the adult form (Fair et al., 2008; Markham & Greenough, 2004). Nevertheless, the degree to which the anatomical and functional changes are coordinated in the developing brain remains sparsely investigated.

To investigate the pattern of structure–function coupling, recent studies took advantage of diffusion tractography to estimate interregional white-matter connectivity and correlated its profile with

This is an open access article under the terms of the Creative Commons Attribution-NonCommercial License, which permits use, distribution and reproduction in any medium, provided the original work is properly cited and is not used for commercial purposes.
© 2022 The Authors. *Human Brain Mapping* published by Wiley Periodicals LLC.

functional connectivity (FC) (Baum et al., 2020; Preti & van de Ville, 2019; Vázquez-Rodríguez et al., 2019). These studies identified a similar pattern of regional variation in which structure and function appear to be tightly coupled in unimodal sensory areas but become systematically decoupled in the supramodal cortex. Despite the strengths of these studies, it should be noted that diffusion tractography has potential limitations to reconstruct the complexity of white-matter pathways accurately. This includes inaccuracies in streamline propagation from angular orientation error, unresolved fibers, or ambiguous orientational information, as well as problems with the tracking process itself through biases, parameter selection, and ambiguities in pathway selection (Schilling et al., 2019; Sotiropoulos & Zalesky, 2019). The regional structure-function coupling was also assessed by computation techniques utilizing structural covariance across populations (Alexander-Bloch et al., 2013). The inter-subject covariance profile of morphological measures, such as CT, resembled FC in a region-specific manner. In addition, cortical myelin content estimated by T1w/T2w ratio is supposed to be more closely related to the underlying microstructure of the gray matter (Ganzetti et al., 2014; Glasser & van Essen, 2011). Accordingly, this has been proposed as an alternative anatomical measure to construct structural covariance networks (Ma & Zhang, 2017; Melie-Garcia et al., 2018). Interestingly, the coupling between myelination covariance and resting-state FC was found to vary across functional networks, with stronger correlation in sensory and motor networks than in cognitive and supramodal association networks (Ma & Zhang, 2017). These results suggest that structure-function relationships might be guided by a hierarchical gradient of cortical information processing spanning unimodal to supramodal cortex (Baum et al., 2020; Paquola et al., 2019; Preti & van de Ville, 2019; Vázquez-Rodríguez et al., 2019), reflected in multiple anatomical, functional, and biochemical markers (Burt et al., 2018; Demirtaş et al., 2019; Felleman & van Essen, 1991; Honey et al., 2012; Margulies et al., 2016; Markov et al., 2014; Murray et al., 2014; Soltani et al., 2021).

Most of the previous neuroimaging studies on structure-function coupling have focused on the adult brains or used diffusion tractography as a measure of structural connectivity, although multiple studies have found reorganization of FC during development (Baum et al., 2020; Dong et al., 2021; Fair et al., 2008). Therefore, how specific patterns of structure-function coupling as observed in the adult human brain, including the parallel changes in structural and functional features along the hierarchy of cortical information processing, emerge during development remains poorly understood. During transition from childhood to adolescence, a gradual shifting of gradient patterns across cortical sheet has been observed (Dong et al., 2021). Nevertheless, whether and how the structure-function coupling and gradient of cortical hierarchy retain their alignment during development remains poorly understood. In the present study, therefore, we investigated the relationship, referred to as meta-correlation (MC), between the resting-state FC and the structural covariance of two anatomical features, namely CT and T1w/T2w ratio, in a cross-sectional cohort of children with ages from 10 to 15.

2 | MATERIALS AND METHODS

2.1 | Participants

Subjects were recruited with an online advertisement, and excluded if they had metal implants, history of substance abuse, previous medical diagnoses, born prematurely under 36 weeks, or if the mother has been using illegal drugs or alcohol for more than 3 months. We obtained structural (T1w and T2w) and resting-state functional MRI (rs-fMRI) scans from a total of 459 adolescent participants. Subjects were excluded based on motion effects in both anatomical and functional data. Anatomical scans were excluded if they failed manual QC from three different researchers. For functional data, subjects were excluded based on their average framewise displacement (FD), computed as the sum of the absolute values of the differentiated realignment estimates (by backwards differences) at every time point (Power et al., 2012). Based on the distribution of mean FD, a value of 0.352 mm was used as the exclusion threshold (corresponding to the distribution mean + 2 SD), which resulted in the removal of 18 subjects. Accordingly, the final dataset analyzed in this study contained 441 subjects (251 males, 190 females, ages 10–15, mean age = 12.3 ± 1.6 years; see Table S1). Data were acquired on two different 3T Siemens Magnetom MRI scanners: a Prisma at Sungkyunkwan University (SKKU; $N = 373$ participants) and a Trio Tim at Seoul National University (SNU; $N = 68$). Subjects were placed in the MRI scanner once prior to the experimental session to introduce them to the scanning environment. The entire procedure was approved by the Public Institutional Review Board (IRB) in the Republic of Korea, and written informed consent was obtained from the parents of each participant.

2.2 | Data acquisition

All structural scans had a field of view (FOV) of 256 mm^2, voxels which are 1.0 mm^3 in size, and acquired using GRAPPA parallel acquisition with a PAT acceleration factor of 2. SKKU T1w scans were acquired using a 3D TurboFLASH sequence with repetition time (TR) = 2400 ms, echo time (TE) = 2.58 ms, flip angle = 12° and total acquisition time of 5 min 43 s. SKKU T2w scans were acquired using a modified variable flip angle 3D Turbo Spin Echo sequence (NATIVE SPACE) with TR = 3200 ms, TE = 352 ms, and total acquisition time of 6 min 19 s. SNU T1w scans were acquired using a 3D TurboFLASH sequence with TR = 2400 ms, TE = 2.68 ms, flip angle = 12° and total acquisition time of 5 min 43 s. SNU T2w scans were acquired using a 3D-Turbo spin-echo sequence with a variable flip-angle (TSE VFL) with TR = 3200 ms, TE = 333 ms, and total acquisition time of 6 min 51 s.

All functional scans at both sites were acquired using an EPI-FID sequence with GRAPPA parallel acquisition with a PAT acceleration factor of 2. SKKU rs-fMRI scans were acquired with TR = 952 ms, TE = 32.0 ms, measurements = 750, FOV = 210 mm^2, multi-band acceleration factor = 4, voxel size = 2.5 mm^3, and total acquisition time of 12 min 13 s. SNU rs-fMRI scans were acquired with

10970193, 2023, 4, Downloaded from https://onlinelibrary.wiley.com/doi/10.1002/hbm.26173 by South Korea National Provision, Wiley Online Library on [04/01/2024]. See the Terms and Conditions (https://onlinelibrary.wiley.com/terms-and-conditions) on Wiley Online Library for rules of use; OA articles are governed by the applicable Creative Commons License

TR = 1400 ms, TE = 35.6 ms, measurements = 500, FOV = 270 mm^2, multi-band acceleration factor = 3, voxel size = 3.2 × 3.2 × 2.5 mm^3, and total acquisition time of 12 min 1 s. Two short (three measurement) spin-echo field map scans, with opposite phase encoding directions, were also acquired for use in distortion correction. Participants were instructed to relax and lay still in the scanner with their eyes open and not to fall asleep.

2.3 | Preprocessing

All our scans were processed using the same processing steps. Structural MRI were processed using the HCP minimal preprocessing pipelines (version 3.22), which consists of the PreFreeSurfer, FreeSurfer, and PostFreeSurfer pipelines (Fischl, 2012; Glasser et al., 2013, 2016). The T1w and T2w images were aligned with the anterior commissure–posterior commissure (AC–PC) line, brain extracted, corrected for intensity bias and registered to the MNI template. The images were then parcellated based on the Schaefer parcellation (a functional parcellation based on resting-state FC data with 400 total regions of interest (ROI); Schaefer et al., 2018), the white and pial surfaces were traced, and the data were projected onto the cortical surface. Standard anatomical measures such as CT, area, volume, and curvature were then computed both on the volume and on the surface. In addition, because gyral crowns tend to be thicker than sulcal fundi, the CT was corrected for folding-related biases by regressing out the mean curvature measure from each subjects' thickness data (Glasser & van Essen, 2011). Myelin content was computed by taking the log ratio of T1w/T2w signal intensities on a voxel-by-voxel basis, on the standard CIFTI grayordinate surface. The log is taken to remove the implicit ratio bias present in any ratio, in order to give equal weights to deviations in the numerator and denominator. Other details of the processing were consistent with those used in previous studies (Fischl, 2012; Glasser et al., 2013).

The resting-state fMRI data were processed with our custom fMRI-volume and fMRI-surface pipelines, which were modeled after the HCP pipeline (version 3.22, Glasser et al., 2013). The fMRI-volume pipeline consisted of temporal de-spiking, motion correction, susceptibility distortion correction (using FSL's TOPUP in conjunction with two spin echo field maps with opposite phase encoding direction; Andersson et al., 2003), brain extraction, slice-timing correction, registration to MNI and anatomical space, volume censoring with interpolation, and voxel-level time series normalization. For the interpolation, the metric used was DVARS thresholded using the boxplot cutoff (75% + 1.5 × IQR), and only the volume in question was censored. In addition, artifacts caused by subject motion, cardiac pulsation, and other spurious sources of noise were further cleaned by the ICA + FIX pipeline (Griffanti et al., 2014; Salimi-Khorshidi et al., 2014). Finally, a temporal band-pass filter of 0.008–0.1 Hz was applied to the resulting time series. The fMRI-surface pipeline takes the processed volumetric data and projects it onto the standard CIFTI grayordinate surface (59,412 voxels), as well as smooths the data with a full width half max of 2 mm.

The anatomical and functional surface maps were then parcellated based on the Schaefer parcellation, which is a functional parcellation based on resting-state FC data with 400 total ROI separated into 17 resting state networks (RSNs; Schaefer et al., 2018). For myelin and CT, the average over all grayordinate voxels in a given ROI was taken as the ROI's value. This process is the same for the functional data, but here mean time series were computed for each ROI from the individual time series of each voxel.

Motion is a known issue for fMRI data, especially for younger subjects (Cosgrove et al., 2022; Power et al., 2012), so we examined the effects of motion in our data. Given that FD was moderately correlated with age ($r = -0.35$, $p < .0001$) in our data, we computed the FD-FC correlation proposed by (Ciric et al., 2017) for each of our Schaefer ROIs. We found that the values of FD-FC correlation were centered around zero without any signs of large motion effects. The absolute median FD-FC correlation was 0.062, which is comparable to the results obtained from the best models used in Ciric et al. (2017) (their Figure 3).

2.4 | Correlation matrices for anatomical features and resting-state FC

Since the current study focuses on local features, global patterns, and correlations were removed in all of our data at the subject level. Demeaning of the myelin and CT measures was done by computing mean myelin and CT across all ROI for each participant and subtracting it from the individual myelin and CT measures of each ROI, respectively. Then, the parcellated data for each participant was stacked into a matrix (441 × 400) and the Pearson correlation across participants was then computed to create ROI-level correlation matrices (400 × 400). For the functional data, global signal regression was performed for each individual, and FC matrices were constructed by taking the Pearson correlation between each region's residual time series. These matrices were then averaged to create a group-averaged ROI-level resting-state FC matrix (400 × 400).

Sex was regressed out of all measures to account for sex differences, and for FC, average root mean square (RMS) motion was also regressed out to account for motion effects. To remove the confounding effects from multi-site data, we also applied an inter-site harmonization procedure to our data via the commonly used tool ComBat (Fortin et al., 2018; Johnson et al., 2007). ComBat removes site effects from measures extracted from processed MRI scans, which in our case are the myelin and CT measures for the anatomical data and the FC measures for the functional. Regression and harmonization of the myelin and CT measures was done prior to cross-subject correlation by operating on the stacked matrices. For the FC data, the upper triangles of each subject's FC matrices were stacked together, regressed, and harmonized, and then re-separated into the original FC matrices prior to group averaging.

Reproducibility of myelination, thickness covariance, and FC was assessed using a split-group approach, in which all 441 subjects were randomly divided into two subgroups (n = 220 and 221). The

10970193, 2023, 4, Downloaded from https://onlinelibrary.wiley.com/doi/10.1002/hbm.26173 by South Korea National Provision, Wiley Online Library on [04/01/2024]. See the Terms and Conditions (https://onlinelibrary.wiley.com/terms-and-conditions) on Wiley Online Library for rules of use; OA articles are governed by the applicable Creative Commons License

covariance matrices were independently computed for each subgroup, and reproducibility was evaluated by Pearson correlation of the corresponding covariance values between the two subgroups. Between-matrices correlations were calculated to evaluate the shared variance and its significance was estimated using the Mantel permutation test.

2.5 | Meta-correlations

In addition to examining the correlation between the anatomical or functional measures of different participants, we also explored the relation between these different correlation matrices. Given two correlation matrices, we can compute the Pearson correlation between each row vector of one matrix and another row vector of the other matrix and obtain a new correlation coefficient matrix, which is herein referred to as MC (Figure 1). We consider three such meta-correlations: myelin-FC meta-correlation (myelin-FC MC), CT-FC meta-correlation (CT-FC MC), and myelin-CT meta-correlation (myelin-CT MC). Reproducibility of MC was assessed using a split-group approach. Both myelin-FC MC and CT-FC MC provide quantitative measures of structural-functional coupling in the cortex. We calculated the spatial correspondence between the two brain maps and assessed to what extent they are aligned. Significance of the MCs were quantified using BrainSMASH (Burt et al., 2020), which was developed for statistical testing of spatially autocorrelated brain measures. This approach is based on matching spatial-autocorrelation variograms between surrogate and target maps. For each ROI, the MC was computed from two corresponding brain measure maps (i.e., rows in the correlation matrices). We generated 1000 surrogate maps with preserved spatial autocorrelation for one of the brain maps. The *p*-value was calculated as the incidence of these surrogate maps having correlations more extreme than original MC. Similar procedure was also performed to assess the significance of the spatial correspondence between different brain maps.

To evaluate the relationship between MC and cortical functional hierarchies (Dong et al., 2021; Margulies et al., 2016), principal gradient of group-averaged FC was computed using BrainSpace (vos de Wael et al., 2020). Briefly, the group-averaged FC matrix was transformed to a nonnegative and symmetric affinity matrix using normalized angle similarity kernels. Then, diffusion map embedding, a nonlinear dimensionality reduction technique, was applied on this affinity matrix to obtain a low-dimensional representation of the FC matrix. The principal gradient that accounts for the greatest variance in connectivity was used as the map to denote the cortical functional hierarchy, and was correlated with MC brain maps.

In order to examine MCs between anatomical correlation and FC, we computed the MC between each ROI of the Schaefer parcellation, as well as between the 17 different RSN into which the Schaefer ROIs are grouped (mean ROI per network = 23.5 ± 8.5). MCs for each of the RSN were computed as the average Fisher's z-transformed MC of all ROI within the network. This was a weighted average, where the weights for each network ROI were the number of voxels in that ROI divided by the total number of voxels in the network. The breakdown of networks and ROI are shown in Figure 2.

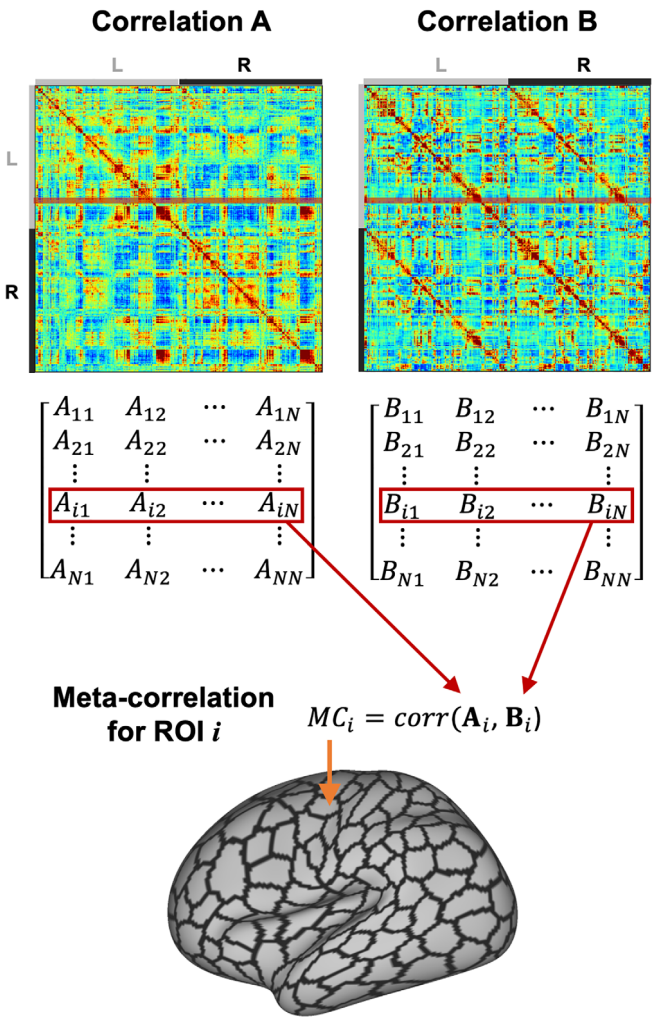

FIGURE 1 Schematic diagram describing the ROI level meta-correlation. At the top level (the correlation matrices), the correlation profile vectors for a given ROI (size 1 × 400) are extracted from each of the matrices. These vectors are then correlated to get a meta-correlation for that region. The type of meta-correlation is determined by the choices of the A and B matrices (myelin, thickness, covariance, or FC).

2.6 | Age dependence of the MC

We examined the effect of age on the MC both within our sample, and in comparison to HCP young adults (van Essen et al., 2013). To test whether the structural correlation in myelin and CT and their MC with FC in our own data might be driven by age-dependent maturational coupling, we recomputed the myelin and CT covariance matrices as well as the MC using the residuals from a regression model in which the effect of age was regressed out from a given anatomical or functional feature.

10970193, 2023, 4, Downloaded from https://onlinelibrary.wiley.com/doi/10.1002/hbm.26173 by South Korea National Provision, Wiley Online Library on [04/01/2024]. See the Terms and Conditions (https://onlinelibrary.wiley.com/terms-and-conditions) on Wiley Online Library for rules of use; OA articles are governed by the applicable Creative Commons License

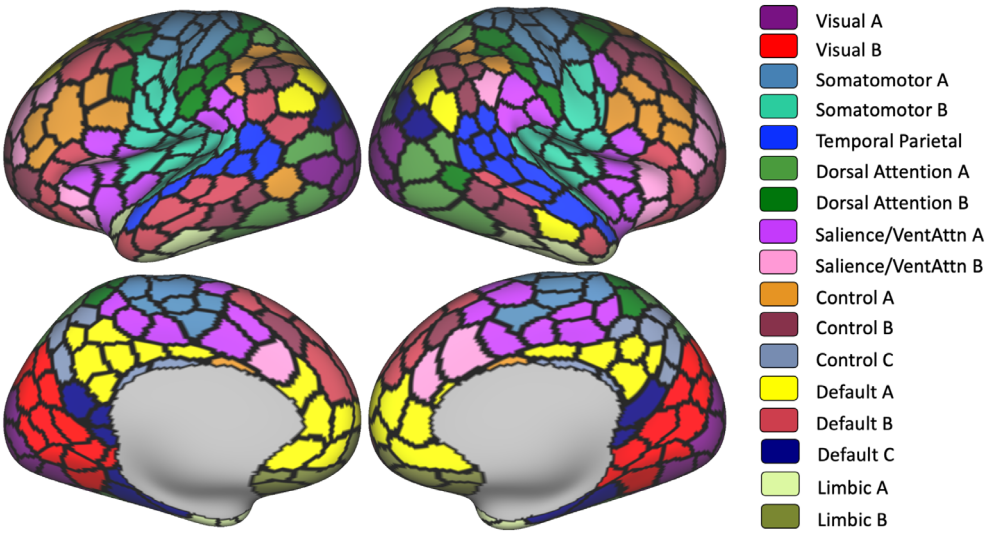

FIGURE 2 Four-hundred ROI's from the Schaefer parcellation, colored according to which of the 17 resting state networks they reside within.

In order to compare our results from adolescents with those from adults, we used data from the Human Connectome Project (HCP) (Glasser et al., 2016; van Essen et al., 2013). Preprocessed myelin brain maps and rs-fMRI time series, which were derived from the HCP minimal preprocessing pipelines, were downloaded for $N = 1113$ subjects (507 male, age 22–37 years) from the HCP S1200 release, for which informed consent was obtained. After excluding subjects whose data were not complete or the FD of rs-fMRI scan exceeds 0.273 mm (same exclusion criteria as used in adolescents data, i.e., average FD plus two times the standard deviation), $N = 1047$ subjects (mean age 28.7 ± 3.7 years) remained. Details in HCP scanning parameters and preprocessing pipeline have been reported elsewhere (Glasser et al., 2013, 2016). Myelin-FC MC was then estimated using the same processing steps mentioned above. Although our experiments followed closely with HCP in terms of scanning protocols and preprocessing steps, there are still some differences remaining that prevent a direct quantitative comparison. Therefore, we used the principal FC gradient derived from RSFC as a reference of cortical organization and assessed whether the spatial correspondence between myelin-FC MC and functional gradient varies from adolescents to adults.

3 | RESULTS

3.1 | Reproducibility of correlation matrices

We first examined the correlation matrices for the myelin and CT as well as the FC matrix (Figure 3). The mean absolute value of ROI correlations revealed that, overall, the correlations were smaller for CT than for myelin and FC ($|r| = 0.155$, 0.062, and 0.126, for myelin, CT, and FC, respectively). In addition, the standard deviations of the correlation values shows that CT has a much lower variability than the other measures ($\sigma = 0.204$, 0.095, and 0.171, for myelin, CT, and FC, respectively). Nevertheless, these measures of correlation and FC were robust as revealed by the correlation coefficient between the two correlation coefficient matrices computed for two randomly divided subgroups. These reproducibility scores were still higher for FC and myelin ($r = 0.99$ and 0.83, respectively) than for CT ($r = 0.49$).

We quantified the overall association among myelin covariance, CT covariance, and FC. Across 79,800 edges between the 400 brain regions, there is a moderate similarity between myelin and CT covariance matrices ($r^2 = 0.25$, Mantel permutation test $p < .001$). There is also a significant association between myelin covariance and FC ($r^2 = 0.19$, Mantel permutation test $p < .001$), and CT covariance and FC ($r^2 = 0.14$, Mantel permutation test $p < .001$), respectively. The association of myelin covariance-FC was significantly stronger than that of CT covariance and FC (Fisher's z method, $p < 10^{-12}$). To assess whether myelin and CT provide similar or distinct structural constraints for FC, multivariate regression was performed. When combined, myelin, and CT covariances can explain up to 22.3% of variance in FC across all pairs of brain regions (Partial Mantel permutation test $p < .001$). The correlation coefficient ($r = 0.47$) was significantly higher than using myelin or CT covariance alone as predictor ($p < 10^{-6}$).

3.2 | Reproducibility and significance of MCs

We explored the relationship between myelin, CT, and FC by computing correlations between the rows of the individual correlation matrices, that is, the MC, for each pair of demeaned measures (see Section 2). This produced ROI level maps for the myelin-FC MC, CT-FC MC, and myelin-CT MC (Figure 4). Among these three MC measures the myelin-CT MC was overall strongest (mean MC = 0.56), followed by the myelin-FC MC (mean MC = 0.50), and the CT-FC MC (mean MC = 0.48). The reproducibility of these MCs was quantified by correlation between two randomly divided subgroups, which were 0.86, 0.57, and 0.67 for the myelin-FC MC, CT-FC MC, and myelin-CT

10970193, 2023, 4, Downloaded from https://onlinelibrary.wiley.com/doi/10.1002/hbm.26173 by South Korea National Provision, Wiley Online Library on [04/01/2024]. See the Terms and Conditions (https://onlinelibrary.wiley.com/terms-and-conditions) on Wiley Online Library for rules of use; OA articles are governed by the applicable Creative Commons License

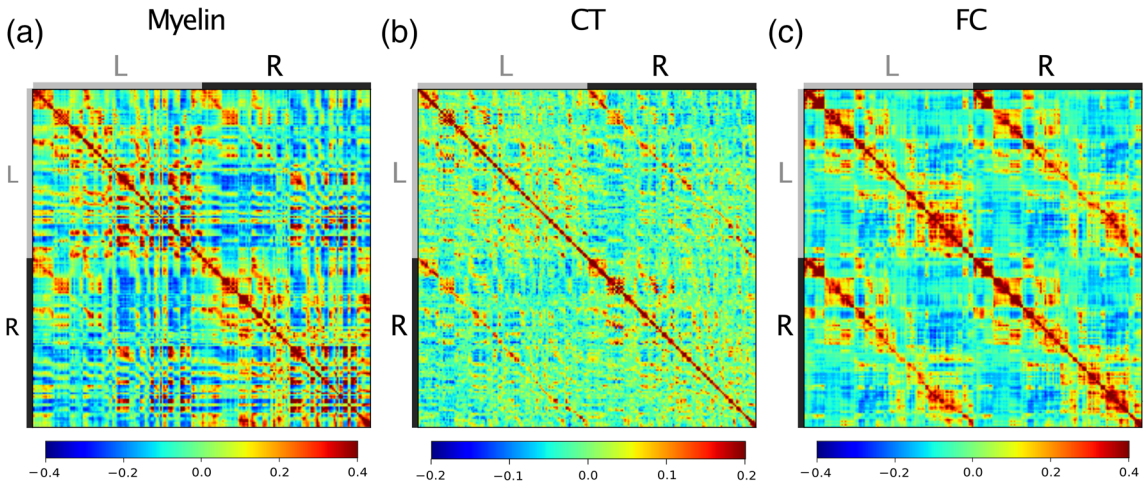

FIGURE 3 Demeaned ROI level correlation matrices for myelin (a), CT (b), and FC (c). The hemisphere is indicated by the L (left) or R (right) at the top/left of the matrices. The ROIs are ordered in the same way in each of the matrices.

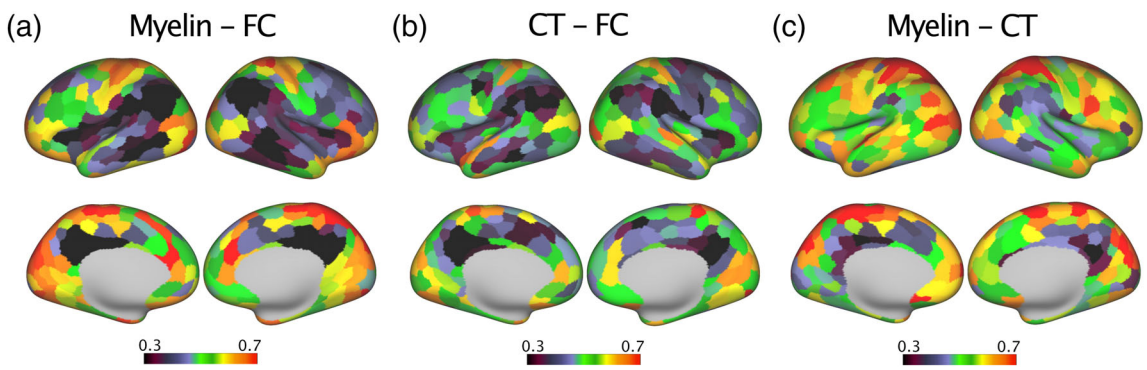

FIGURE 4 ROI-level meta-correlation maps for myelin-FC (a), CT-FC (b), and myelin-CT (c).

MC, respectively. These results indicate that myelin-FC MC is the most robust of the three measures, while myelin-CT MC is the least.

Across all three types of MC, the superior parietal regions around the central sulcus and occipital regions tended to display largest MC values, while the area around the precuneus contains uniformly small MC. For the myelin-FC and myelin-CT MC, some areas of the medial frontal regions also showed large values. The myelin-FC MC map also shows higher values in the occipital lobe.

Next, we tested whether these regional variations in the MC might merely reflect the spatial autocorrelations in the underlying matrices. The resulting brain maps of *p*-value (Figure 5) show that brain regions with high MCs are statistically significant even when spatial autocorrelations were accounted for (spatial-autocorrelation preserved null hypothesis testing, $p_{SA} < .05$). There is also a strong correlation between myelin-FC MC and CT-FC MC brain maps ($r = 0.68$, Figure 6), indicating the consistency of the two structural-functional coupling measures. This correlation remains statistically significant after accounting for spatial autocorrelation ($p_{SA} < .001$). However, it should be noted that CT-FC MC overall shows lower correlations and narrower dynamic range compared to myelin-FC MC.

3.3 | Strength of resting state network MCs

In order to obtain more robust measures of MC and characterize their patterns at a network level, we computed the average z-transformed MC of all ROIs within each of the 17 Schaefer networks for each MC (Figure 7). The MC for the somatomotor-A network showed the largest value for myelin-FC and myelin-CT MC, and also was the only network with larger than average MCs for all three MCs. The highest single MC value was for the myelin-CT MC of the somatomotor-A network (MC = 0.82), while the lowest was the myelin-FC MC of the default-A network (MC = 0.38).

3.4 | Minimal age-related effects on MCs

To examine the linear effect of age on MC, we compared the MCs before and after regressing out the age-related changes in myelin, CT, and FC out of each ROI (Figure 8). We found that the MCc were largely unaffected by regressing out the age-related changes ($r > 0.98$).

10970193, 2023, 4, Downloaded from https://onlinelibrary.wiley.com/doi/10.1002/hbm.26173 by South Korea National Provision, Wiley Online Library on [04/01/2024]. See the Terms and Conditions (https://onlinelibrary.wiley.com/terms-and-conditions) on Wiley Online Library for rules of use; OA articles are governed by the applicable Creative Commons License

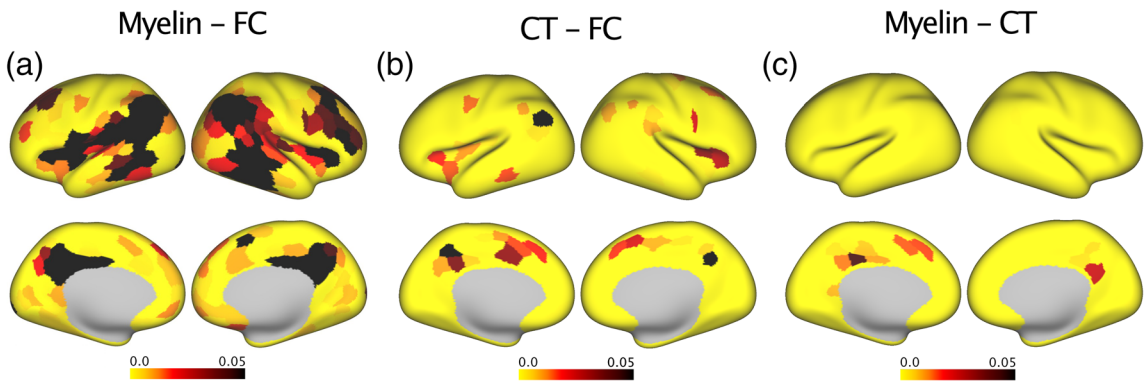

FIGURE 5 ROI-level maps of significant MC after accounting for spatial autocorrelation for myelin-FC (a), CT-FC (b), and myelin-CT (c). The *p*-value is indicated by the color, where black represents *p*-values >.05.

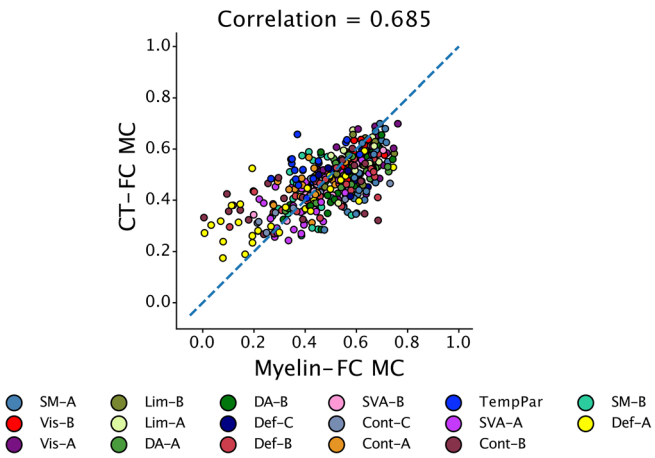

FIGURE 6 Plots of myelin-FC MC versus CT-FC MC for each Schaefer ROI. The overall Pearson correlation between them is shown at the top. The ROIs have been colored according to network, and the color key is shown at the bottom.

3.5 | Regional variability in myelin-FC MC reflects cortical hierarchies of functional specialization

It has been shown that principal gradient of FC revealed by the diffusion embedding method captures a primary dimension of variance in FC from unimodal sensory areas to supramodal association regions (Margulies et al., 2016). The principal gradient derived from our adolescents' FC data (Figure 9a) showed consistent functional hierarchies, in which one end is anchored at visual, somatomotor, and auditory regions, and the other end spans default mode network regions. We evaluated whether regional variability in the MCs reflect such a macroscale functional hierarchy. For myelin-FC MC, we found that its regional variability aligns significantly with the principal gradient of FC (Figure 9b). We observed stronger MCs in unimodal sensory regions and weaker MCs in association areas ($r = -0.38$, $p_{SA} < .001$). For CT-FC MC, its association with principal FC gradient was lower but still significant ($r = -0.25$, $p_{SA} = .009$).

To test whether myelin-FC MC in the adult brain is similarly related to the principal FC gradient, we performed the same analysis for the results from HCP young adults. The principal FC gradient showed a spatial profile similar to that of adolescents (Figure 9c). In addition, as in the adolescents, the spatial profile of myelin-FC MC again showed significant negative association with principal FC gradient ($r = -0.47$, $p_{SA} < .001$; Figure 9d), and this pattern was not significantly different from that seen in the adolescents (Fisher's z method, $p = .06$).

4 | DISCUSSION

This study investigated the relationship, referred to as MC, between the resting-state FC and the covariance structure of anatomical features, such as the CT and T1w/T2w ratio in children with ages from 10 to 15. We showed that there is a notable consistency in spatial pattern between myelin-FC and CT-FC MCs. In addition, the regional variability of this MC paralleled the cortical hierarchy of functional specialization, with higher coupling in the unimodal sensory cortex and lower coupling in supramodal association regions. Finally, by reproducing the association between MC and function gradient in an independent dataset, we validated our findings and showed that the association persists from adolescence to adulthood.

4.1 | Microstructural versus macrostructural correlation

As shown in previous studies, brain structure, such as gray matter volume and CT, varies across the population in a coordinated fashion. Brain regions that belong to the same functional group often covary in their morphological properties. For example, CT of brain regions that are connected structurally and functionally tend to covary (Alexander-Bloch et al., 2013; Gong et al., 2012). The architecture of CT-based structural correlation has also been shown to be genetically heritable (Pol et al., 2006; Schmitt et al., 2008) and is associated with behavioral and cognitive abilities (Bermudez et al., 2009; Carreiras et al., 2009). As myeloarchitecture can now be reliably estimated with MR, we examined in the present study how CT and FC might be

10970193, 2023, 4, Downloaded from https://onlinelibrary.wiley.com/doi/10.1002/hbm.26173 by South Korea National Provision, Wiley Online Library on [04/01/2024]. See the Terms and Conditions (https://onlinelibrary.wiley.com/terms-and-conditions) on Wiley Online Library for rules of use; OA articles are governed by the applicable Creative Commons License

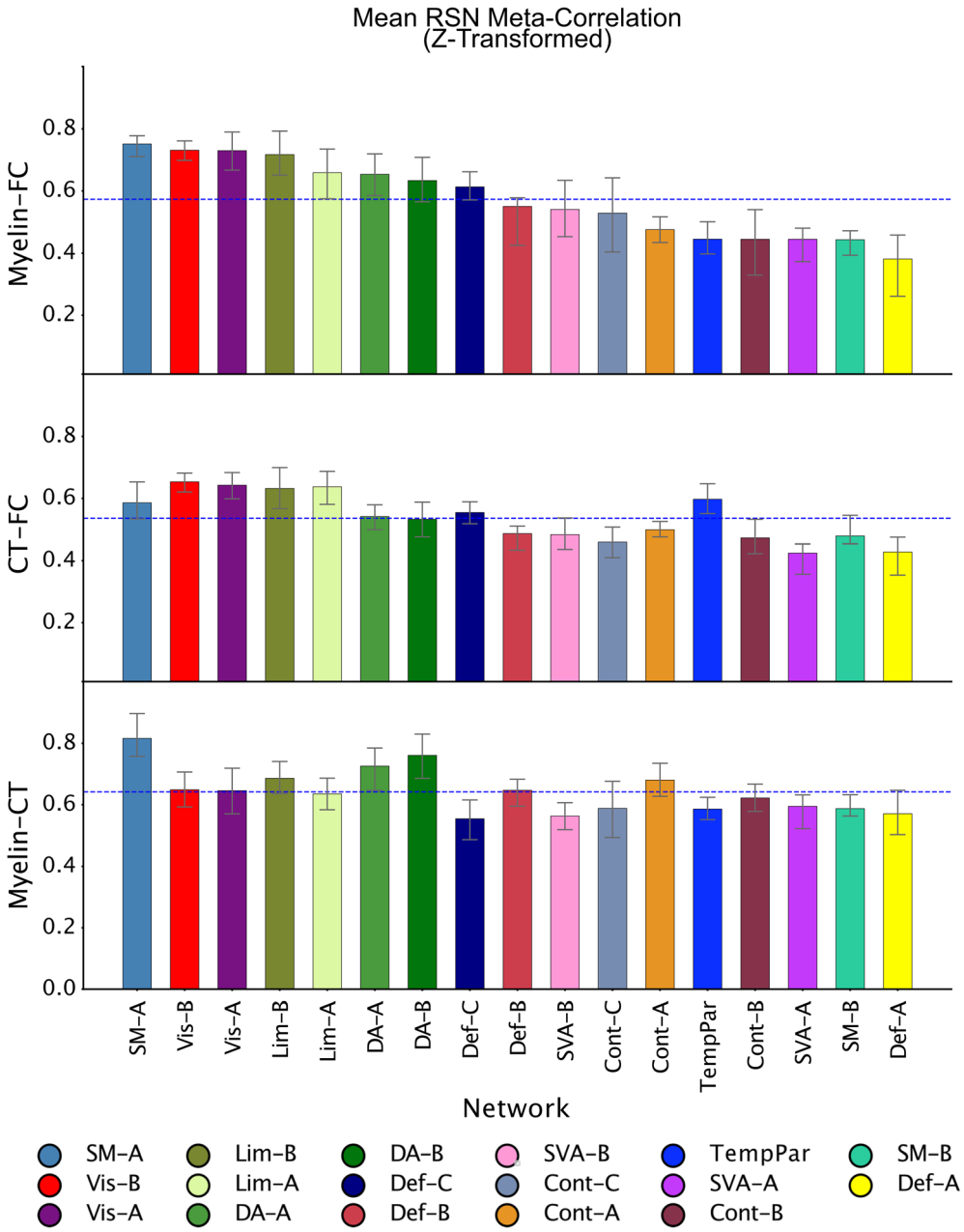

FIGURE 7 Mean z-transformed resting state network meta-correlations for the 17 Schaefer networks. The order of networks in all plots was determined by the values of myelin-FC MC (top). The global mean of all networks is indicated by the blue dashed line in each panel. Error bars represent 95% confidence intervals computed using weighted bootstrapping with 1000 samples.

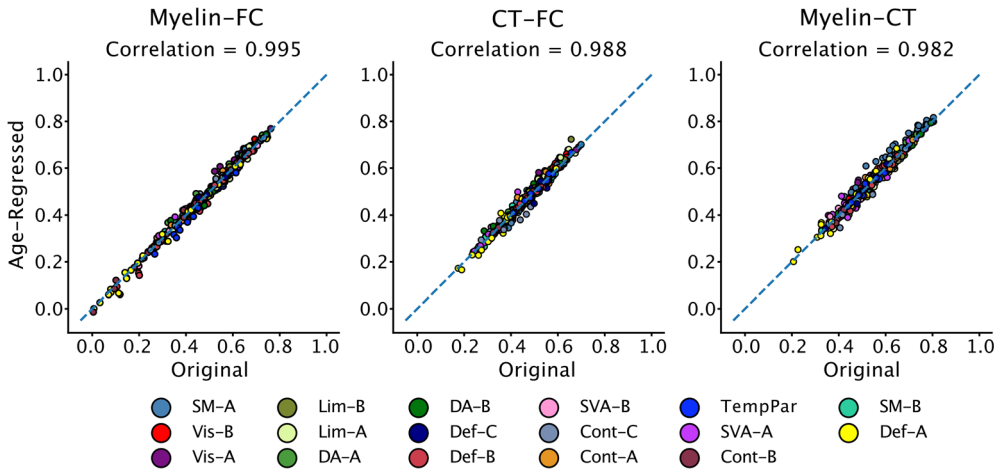

FIGURE 8 Plots of original versus age-regressed myelin-FC MC (left), CT-FC MC (middle) and myelin-CT MC (right) for each Schaefer ROI. The overall Pearson correlation between them is indicated above each plot. The ROIs have been colored according to network as in Figure 6.

10970193, 2023, 4, Downloaded from https://onlinelibrary.wiley.com/doi/10.1002/hbm.26173 by South Korea National Provision, Wiley Online Library on [04/01/2024]. See the Terms and Conditions (https://onlinelibrary.wiley.com/terms-and-conditions) on Wiley Online Library for rules of use; OA articles are governed by the applicable Creative Commons License

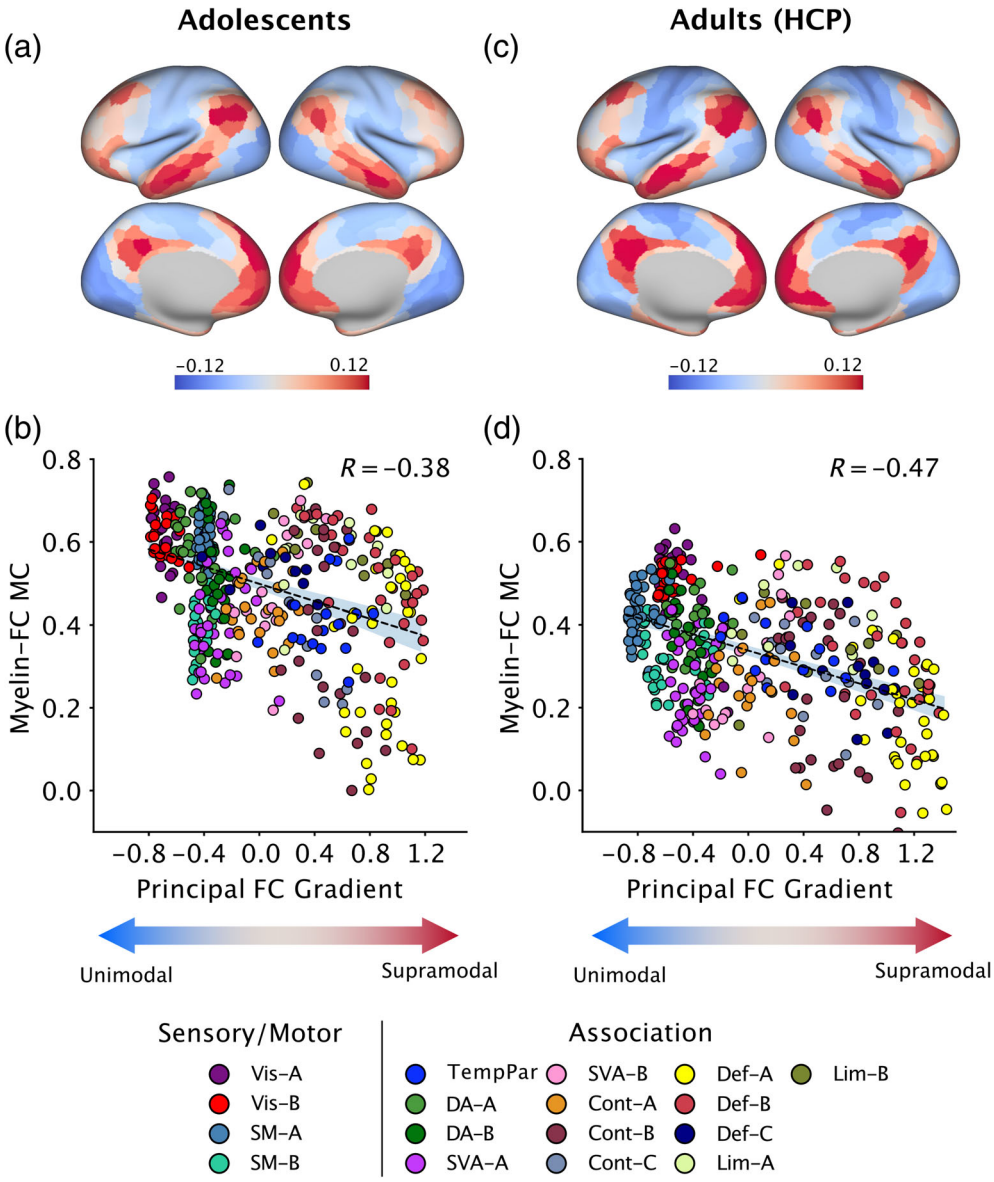

FIGURE 9 The principal gradient of the FC matrix (a) that shows the functional hierarchies of unimodal (blue) and supramodal (red) regions, and the scatter plot of myelin-FC MC versus principal FC gradient for adolescents (mean age 12.3 ± 1.6 years) (b). For comparison, the principal FC gradient of HCP young adults (mean age 28.7 ± 3.7 years) (c), and its association with myelin-FC MC (d) are also shown. The overall Pearson correlation between them is shown above the plot. The ROIs have been colored according to the network, as in Figure 6.

linked to myelin covariance matrix. The higher correlation coefficients and reproducibility in myelin covariance, as shown in the present study, indicates the higher level of synchronized cortical myelination might better reflect the FC between region pairs than morphological measures. Whereas the biological significance of the structural covariance remains incompletely understood, the markedly stronger correlation found in cortical myelination might still contain useful information that reflect developmental coordination or synchronized maturation between different areas of the brain.

In addition, we showed that the myelin covariance accounts for more variability in FC than CT covariance does. Even more variance of FC can be explained when including both myelin and CT covariance as predictors. Thus, both myelin and CT covariances provide consistent and complementary information of the structural substrate for brain functions. Note that our estimation of myelin was based upon the T1w/T2w ratio. Although the T1w/T2w ratio does not correspond to cortical myelin density in a one-to-one fashion (Arshad et al., 2017; Hagiwara et al., 2018; Uddin et al., 2019), it is still a useful marker of myelination. Consistent with previous studies (Glasser & van Essen, 2011), our results also show that the highest myelin density occurs in sensorimotor and visual cortices.

4.2 | MCs between structural covariance and function connectivity

Our results indicate that coordinated myelination between brain regions is related to FC (Alexander-Bloch et al., 2013; Huntenburg et al., 2017). By carrying out the brain-wide meta-correlation analysis of structural-functional relationship, we demonstrated the association between the FC and the structural correlation. We also characterized the spatially heterogeneous nature of the MC, where unimodal sensory networks, including somatomotor and visual network regions, consistently showed higher values than supramodal association

10970193, 2023, 4, Downloaded from https://onlinelibrary.wiley.com/doi/10.1002/hbm.26173 by South Korea National Provision, Wiley Online Library on [04/01/2024]. See the Terms and Conditions (https://onlinelibrary.wiley.com/terms-and-conditions) on Wiley Online Library for rules of use; OA articles are governed by the applicable Creative Commons License

networks. These results were also consistent with the patterns observed between FC and structural covariance based on diffusion-weighted imaging (Baum et al., 2020; Vázquez-Rodríguez et al., 2019). These results raise the possibility that the maturation of myelin might be closely coordinated with developmental changes in the organization of FC during adolescence. Our findings also reveal a high spatial correspondence between myelin-FC and CT-FC MCs. This consistency indicates that the coordinated structural-functional development is reflected in both morphological and microstructural measures.

We also demonstrated that the myelin-FC MC shares similar spatial patterns with cortical hierarchies of functional specialization (Baum et al., 2020; Burt et al., 2018). The convergence of myelin covariance profiles and FC in unimodal sensory regions suggests that the FC in these brain areas might be strongly determined by direct anatomical connections between them. In contrast, the relatively lower MCs in supramodal regions indicate the FC is less coupled with structural connectivity and may rely on indirect pathways to transmit neural signals.

The fact that the spatial correspondence between myelin-FC MC and functional gradient can be reproduced in an independent dataset demonstrates the robustness of the relationship. In addition, this association remains at a similar level in both adolescents and young adults. MC measures the similarity between structural and functional correlation profiles across the brain, so myelin-FC MC can be used as an index of myelin-FC coupling. Although the age-group comparison in this study remains qualitative due to the differences in data acquisition and processing, the persistent association between myelin-FC MC and functional gradient implies an age-independent mechanism underpinning the coordinated anatomical and functional changes during brain maturation.

Several limitations of the current study should be noted. First, our focused age range (10–15 years) suits group-level analysis due to the homogeneity of the cohort, but limits the statistical power of age-effect analysis presented above. Also, the reliable construction of structural covariance (i.e., myelin and CT covariance matrix) requires a large group of subjects and precludes investigating how MC changes over the age range of current study. Second, age-associated motion artifacts in both anatomical and rs-fMRI can be a concern when interpreting our results (Cosgrove et al., 2022; Power et al., 2012). We instituted several procedures to mitigate the effect of motion in rs-fMRI, such as exclusion of data with excessive motion, ICA-based denoising, and the use of motion regressors in our analysis. Note that only group-averaged FC is used when estimating MCs which further reduces the motion artifacts. Finally, our findings are derived from a cross-sectional study. To further improve our understanding in association between myelination and FC, it would be beneficial to conduct longitudinal assessment of the measures discussed in this study and such data are currently being collected in the ABCD study (Chaarani et al., 2021). Previous studies using CT-based correlation network analysis have shown that correlated anatomical structure between brain regions results from similarities in maturational trajectories (Alexander-Bloch et al., 2013; Khundrakpam et al., 2019).

In conclusion, by quantifying the regional coupling between resting-state FC and structural covariance, we observed the MCs related to CT and T1w/T2w ratio share a consistent pattern which markedly aligns with cortical hierarchy of functional specialization. We validated our findings by reproducing the association between MC and function gradient in an independent dataset from young adults, and showed that the association persists from adolescence to adulthood.

ACKNOWLEDGMENTS

We thank Zhiwei Ma and Nanyin Zhang for the helpful discussion. This work was supported by Neurogazer Inc.

CONFLICT OF INTEREST

The authors declare that they have known competing financial interests or personal relationships that could have appeared to influence the work reported in this article, as some are employees of Neurogazer Inc. which also funded this study.

DATA AVAILABILITY STATEMENT

The authors have made the final numerical values used to make all figures in the current study, along with the code to generate them, available for the public via a GitHub repository: https://github.com/neurogazer-usa/PAFA.git.

PATIENT CONSENT STATEMENT

The authors received written informed consent from the parents or legal guardians of all subjects recruited for this study.

ORCID

Daeyeol Lee https://orcid.org/0000-0003-3474-019X

REFERENCES

Alexander-Bloch, A., Raznahan, A., Bullmore, E., & Giedd, J. (2013). The convergence of maturational change and structural covariance in human cortical networks. *The Journal of Neuroscience*, *33*, 2889–2899.

Andersson, J. L. R., Skare, S., & Ashburner, J. (2003). How to correct susceptibility distortions in spin-echo echo-planar images: Application to diffusion tensor imaging. *NeuroImage*, *20*, 870–888.

Arshad, M., Stanley, J. A., & Raz, N. (2017). Test-retest reliability and concurrent validity of in vivo myelin content indices: Myelin water fraction and calibrated T_1w/T_2 w image ratio: Test-retest reliability and concurrent validity of in vivo myelin content indices. *Human Brain Mapping*, *38*, 1780–1790.

Baum, G. L., Cui, Z., Roalf, D. R., Ciric, R., Betzel, R. F., Larsen, B., Cieslak, M., Cook, P. A., Xia, C. H., Moore, T. M., Ruparel, K., Oathes, D. J., Alexander-Bloch, A. F., Shinohara, R. T., Raznahan, A., Gur, R. E., Gur, R. C., Bassett, D. S., & Satterthwaite, T. D. (2020). Development of structure–function coupling in human brain networks during youth. *Proceedings of the National Academy of Sciences*, *117*, 771–778.

Bermudez, P., Lerch, J. P., Evans, A. C., & Zatorre, R. J. (2009). Neuroanatomical correlates of musicianship as revealed by cortical thickness and voxel-based morphometry. *Cerebral Cortex*, *19*, 1583–1596.

Burt, J. B., Demirtaş, M., Eckner, W. J., Navejar, N. M., Ji, J. L., Martin, W. J., Bernacchia, A., Anticevic, A., & Murray, J. D. (2018). Hierarchy of transcriptomic specialization across human cortex captured by structural neuroimaging topography. *Nature Neuroscience*, *21*, 1251–1259.

Burt, J. B., Helmer, M., Shinn, M., Anticevic, A., & Murray, J. D. (2020). Generative modeling of brain maps with spatial autocorrelation. *NeuroImage*, *220*, 117038.

10970193, 2023, 4, Downloaded from https://onlinelibrary.wiley.com/doi/10.1002/hbm.26173 by South Korea National Provision, Wiley Online Library on [04/01/2024]. See the Terms and Conditions (https://onlinelibrary.wiley.com/terms-and-conditions) on Wiley Online Library for rules of use; OA articles are governed by the applicable Creative Commons License

Carreiras, M., Seghier, M. L., Baquero, S., Estévez, A., Lozano, A., Devlin, J. T., & Price, C. J. (2009). An anatomical signature for literacy. *Nature*, *461*, 983–986.

Chaarani, B., Hahn, S., Allgaier, N., Adise, S., Owens, M. M., Juliano, A. C., Yuan, D. K., Loso, H., Ivanciu, A., Albaugh, M. D., Dumas, J., Mackey, S., Laurent, J., Ivanova, M., Hagler, D. J., Cornejo, M. D., Hatton, S., Agrawal, A., Aguinaldo, L., … Garavan, H. P. (2021). Baseline brain function in the preadolescents of the ABCD Study. *Nature Neuroscience*, *24*, 1176–1186.

Ciric, R., Wolf, D. H., Power, J. D., Roalf, D. R., Baum, G. L., Ruparel, K., Shinohara, R. T., Elliott, M. A., Eickhoff, S. B., Davatzikos, C., Gur, R. C., Gur, R. E., Bassett, D. S., & Satterthwaite, T. D. (2017). Benchmarking of participant-level confound regression strategies for the control of motion artifact in studies of functional connectivity. *NeuroImage*, *154*, 174–187.

Cosgrove, K. T., McDermott, T. J., White, E. J., Mosconi, M. W., Thompson, W. K., Paulus, M. P., Cardenas-Iniguez, C., & Aupperle, R. L. (2022). Limits to the generalizability of resting-state functional magnetic resonance imaging studies of youth: An examination of ABCD Study® baseline data. *Brain Imaging and Behavior*, *16*, 1919–1925.

Demirtaş, M., Burt, J. B., Helmer, M., Ji, J. L., Adkinson, B. D., Glasser, M. F., van Essen, D. C., Sotiropoulos, S. N., Anticevic, A., & Murray, J. D. (2019). Hierarchical heterogeneity across human cortex shapes large-scale neural dynamics. *Neuron*, *101*, 1181–1194.e13.

Dong, H.-M., Margulies, D. S., Zuo, X.-N., & Holmes, A. J. (2021). Shifting gradients of macroscale cortical organization mark the transition from childhood to adolescence. *Proceedings of the National Academy of Sciences*, *118*, e2024448118.

Fair, D. A., Cohen, A. L., Dosenbach, N. U. F., Church, J. A., Miezin, F. M., Barch, D. M., Raichle, M. E., Petersen, S. E., & Schlaggar, B. L. (2008). The maturing architecture of the brain's default network. *Proceedings of the National Academy of Sciences*, *105*, 4028–4032.

Felleman, D. J., & van Essen, D. C. (1991). Distributed hierarchical processing in the primate cerebral cortex. *Cereb Cortex*, *1*, 1–47.

Fischl, B. (2012). FreeSurfer. *NeuroImage*, *62*, 774–781.

Fortin, J. P., Cullen, N., Sheline, Y. I., Taylor, W. D., Aselcioglu, I., Cook, P. A., Adams, P., Cooper, C., Fava, M., McGrath, P. J., McInnis, M., Phillips, M. L., Trivedi, M. H., Weissman, M. M., & Shinohara, R. T. (2018). Harmonization of cortical thickness measurements across scanners and sites. *NeuroImage*, *167*, 104–120.

Ganzetti, M., Wenderoth, N., & Mantini, D. (2014). Whole brain myelin mapping using T1- and T2-weighted MR imaging data. *Frontiers in Human Neuroscience*, *8*, 671.

Glasser, M. F., Smith, S. M., Marcus, D. S., Andersson, J. L. R., Auerbach, E. J., Behrens, T. E. J., Coalson, T. S., Harms, M. P., Jenkinson, M., Moeller, S., Robinson, E. C., Sotiropoulos, S. N., Xu, J., Yacoub, E., Ugurbil, K., & van Essen, D. C. (2016). The Human Connectome project's neuroimaging approach. *Nature Neuroscience*, *19*, 1175–1187.

Glasser, M. F., Sotiropoulos, S. N., Wilson, J. A., Coalson, T. S., Fischl, B., Andersson, J. L., Xu, J., Jbabdi, S., Webster, M., Polimeni, J. R., van Essen, D. C., & Jenkinson, M. (2013). The minimal preprocessing pipelines for the Human Connectome Project. *NeuroImage*, *80*, 105–124.

Glasser, M. F., & van Essen, D. C. (2011). Mapping human cortical areas in vivo based on myelin content as revealed by T1- and T2-weighted MRI. *The Journal of Neuroscience*, *31*, 11597–11616.

Gong, G., He, Y., Chen, Z. J., & Evans, A. C. (2012). Convergence and divergence of thickness correlations with diffusion connections across the human cerebral cortex. *NeuroImage*, *59*, 1239–1248.

Griffanti, L., Salimi-Khorshidi, G., Beckmann, C. F., Auerbach, E. J., Douaud, G., Sexton, C. E., Zsoldos, E., Ebmeier, K. P., Filippini, N., Mackay, C. E., Moeller, S., Xu, J., Yacoub, E., Baselli, G., Ugurbil, K., Miller, K. L., & Smith, S. M. (2014). ICA-based artefact and accelerated fMRI acquisition for improved Resting State Network imaging. *NeuroImage*, *95*, 232–247.

Grydeland, H., Walhovd, K. B., Tamnes, C. K., Westlye, L. T., & Fjell, A. M. (2013). Intracortical myelin links with performance variability across the human lifespan: Results from T1- and T2-weighted MRI myelin mapping and diffusion tensor imaging. *The Journal of Neuroscience*, *33*, 18618–18630.

Hagiwara, A., Hori, M., Kamagata, K., Warntjes, M., Matsuyoshi, D., Nakazawa, M., Ueda, R., Andica, C., Koshino, S., Maekawa, T., Irie, R., Takamura, T., Kumamaru, K. K., Abe, O., & Aoki, S. (2018). Myelin measurement: Comparison between simultaneous tissue relaxometry, magnetization transfer saturation index, and T1w/T2w ratio methods. *Scientific Reports*, *8*, 10554.

Honey, C. J., Thesen, T., Donner, T. H., Silbert, L. J., Carlson, C. E., Devinsky, O., Doyle, W. K., Rubin, N., Heeger, D. J., & Hasson, U. (2012). Slow cortical dynamics and the accumulation of information over long timescales. *Neuron*, *76*, 423–434.

Huntenburg, J. M., Bazin, P.-L., Goulas, A., Tardif, C. L., Villringer, A., & Margulies, D. S. (2017). A systematic relationship between functional connectivity and intracortical myelin in the human cerebral cortex. *Cerebral Cortex*, *27*, 981–997.

Huttenlocher, P. R. (1979). Synaptic density in human frontal cortex–developmental changes and effects of aging. *Brain Research*, *163*, 195–205.

Johnson, W. E., Li, C., & Rabinovic, A. (2007). Adjusting batch effects in microarray expression data using empirical Bayes methods. *Biostatistics*, *8*, 118–127.

Khundrakpam, B. S., Lewis, J. D., Jeon, S., Kostopoulos, P., Itturia Medina, Y., Chouinard-Decorte, F., & Evans, A. C. (2019). Exploring individual brain variability during development based on patterns of maturational coupling of cortical thickness: A longitudinal MRI study. *Cerebral Cortex*, *29*, 178–188.

Ma, Z., & Zhang, N. (2017). Cross-population myelination covariance of human cerebral cortex: Myelination covariance of cerebral cortex. *Human Brain Mapping*, *38*, 4730–4743.

Margulies, D. S., Ghosh, S. S., Goulas, A., Falkiewicz, M., Huntenburg, J. M., Langs, G., Bezgin, G., Eickhoff, S. B., Castellanos, F. X., Petrides, M., Jefferies, E., & Smallwood, J. (2016). Situating the default-mode network along a principal gradient of macroscale cortical organization. *Proceedings of the National Academy of Sciences*, *113*, 12574–12579.

Markham, J. A., & Greenough, W. T. (2004). Experience-driven brain plasticity: Beyond the synapse. *Neuron Glia Biology*, *1*, 351–363.

Markov, N. T., Ercsey-Ravasz, M. M., Ribeiro Gomes, A. R., Lamy, C., Magrou, L., Vezoli, J., Misery, P., Falchier, A., Quilodran, R., Gariel, M. A., Sallet, J., Gamanut, R., Huissoud, C., Clavagnier, S., Giroud, P., Sappey-Marinier, D., Barone, P., Dehay, C., Toroczkai, Z., … Kennedy, H. (2014). A weighted and directed interareal connectivity matrix for macaque cerebral cortex. *Cerebral Cortex*, *24*, 17–36.

Melie-Garcia, L., Slater, D., Ruef, A., Sanabria-Diaz, G., Preisig, M., Kherif, F., Draganski, B., & Lutti, A. (2018). Networks of myelin covariance. *Human Brain Mapping*, *39*, 1532–1554.

Murray, J. D., Bernacchia, A., Freedman, D. J., Romo, R., Wallis, J. D., Cai, X., Padoa-Schioppa, C., Pasternak, T., Seo, H., Lee, D., & Wang, X.-J. (2014). A hierarchy of intrinsic timescales across primate cortex. *Nature Neuroscience*, *17*, 1661–1663.

Natu, V. S., Gomez, J., Barnett, M., Jeska, B., Kirilina, E., Jaeger, C., Zhen, Z., Cox, S., Weiner, K. S., Weiskopf, N., & Grill-Spector, K. (2019). Apparent thinning of human visual cortex during childhood is associated with myelination. *Proceedings of the National Academy of Sciences*, *116*, 20750–20759.

Paquola, C., Wael, R. V. D., Wagstyl, K., Bethlehem, R. A. I., Hong, S.-J., Seidlitz, J., Bullmore, E. T., Evans, A. C., Misic, B., Margulies, D. S., Smallwood, J., & Bernhardt, B. C. (2019). Microstructural and functional gradients are increasingly dissociated in transmodal cortices. *PLoS Biology*, *17*, e3000284.

Pol, H. E. H., Schnack, H. G., Posthuma, D., Mandl, R. C. W., Baaré, W. F., van Oel, C., van Haren, N. E., Collins, D. L., Evans, A. C., Amunts, K., Bürgel, U., Zilles, K., de Geus, E., Boomsma, D. I., & Kahn, R. S. (2006).

10970193, 2023, 4, Downloaded from https://onlinelibrary.wiley.com/doi/10.1002/hbm.26173 by South Korea National Provision, Wiley Online Library on [04/01/2024]. See the Terms and Conditions (https://onlinelibrary.wiley.com/terms-and-conditions) on Wiley Online Library for rules of use; OA articles are governed by the applicable Creative Commons License

Genetic contributions to human brain morphology and intelligence. *The Journal of Neuroscience*, *26*, 10235–10242.

Power, J. D., Barnes, K. A., Snyder, A. Z., Schlaggar, B. L., & Petersen, S. E. (2012). Spurious but systematic correlations in functional connectivity MRI networks arise from subject motion. *NeuroImage*, *59*, 2142–2154.

Preti, M. G., & van de Ville, D. (2019). Decoupling of brain function from structure reveals regional behavioral specialization in humans. *Nature Communications*, *10*, 4747.

Salimi-Khorshidi, G., Douaud, G., Beckmann, C. F., Glasser, M. F., Griffanti, L., & Smith, S. M. (2014). Automatic denoising of functional MRI data: Combining independent component analysis and hierarchical fusion of classifiers. *NeuroImage*, *90*, 449–468.

Schaefer, A., Kong, R., Gordon, E. M., Laumann, T. O., Zuo, X.-N., Holmes, A. J., Eickhoff, S. B., & Yeo, B. T. T. (2018). Local-global parcellation of the human cerebral cortex from intrinsic functional connectivity MRI. *Cerebral Cortex*, *28*, 3095–3114.

Schilling, K. G., Daducci, A., Maier-Hein, K., Poupon, C., Houde, J.-C., Nath, V., Anderson, A. W., Landman, B. A., & Descoteaux, M. (2019). Challenges in diffusion MRI tractography—Lessons learned from international benchmark competitions. *Magnetic Resonance Imaging*, *57*, 194–209.

Schmitt, J. E., Lenroot, R. K., Wallace, G. L., Ordaz, S., Taylor, K. N., Kabani, N., Greenstein, D., Lerch, J. P., Kendler, K. S., Neale, M. C., & Giedd, J. N. (2008). Identification of genetically mediated cortical networks: A multivariate study of pediatric twins and siblings. *Cereb Cortex*, *18*, 1737–1747.

Selemon, L. D. (2013). A role for synaptic plasticity in the adolescent development of executive function. *Translational Psychiatry*, *3*, e238.

Soltani, A., Murray, J. D., Seo, H., & Lee, D. (2021). Timescales of cognition in the brain. *Current Opinion in Behavioral Sciences*, *41*, 30–37.

Sotiropoulos, S. N., & Zalesky, A. (2019). Building connectomes using diffusion MRI: Why, how and but. *NMR in Biomedicine*, *32*, e3752.

Tau, G. Z., & Peterson, B. S. (2010). Normal development of brain circuits. *Neuropsychopharmacology*, *35*, 147–168.

Uddin, M. N., Figley, T. D., Solar, K. G., Shatil, A. S., & Figley, C. R. (2019). Comparisons between multi-component myelin water fraction, T1w/T2w ratio, and diffusion tensor imaging measures in healthy human brain structures. *Scientific Reports*, *9*, 2500.

van Essen, D. C., Smith, S. M., Barch, D. M., Behrens, T. E. J., Yacoub, E., Ugurbil, K., & WU-Minn HCP Consortium. (2013). The WU-Minn human connectome project: An overview. *NeuroImage*, *80*, 62–79.

Vázquez-Rodríguez, B., Suárez, L. E., Markello, R. D., Shafiei, G., Paquola, C., Hagmann, P., van den Heuvel, M. P., Bernhardt, B. C., Spreng, R. N., & Misic, B. (2019). Gradients of structure–function tethering across neocortex. *Proceedings of the National Academy of Sciences*, *116*, 21219–21227.

vos de Wael, R., Benkarim, O., Paquola, C., Lariviere, S., Royer, J., Tavakol, S., Xu, T., Hong, S. J., Langs, G., Valk, S., Misic, B., Milham, M., Margulies, D., Smallwood, J., & Bernhardt, B. C. (2020). BrainSpace: A toolbox for the analysis of macroscale gradients in neuroimaging and connectomics datasets. *Communicatons Biology*, *3*, 1–10.

SUPPORTING INFORMATION

Additional supporting information can be found online in the Supporting Information section at the end of this article.

How to cite this article: Bero, J., Li, Y., Kumar, A., Humphries, C., Nag, S., Lee, H., Ahn, W. Y., Hahn, S., Constable, R. T., Kim, H., & Lee, D. (2023). Coordinated anatomical and functional variability in the human brain during adolescence. *Human Brain Mapping*, *44*(4), 1767–1778. https://doi.org/10.1002/hbm.26173

10970193, 2023, 4, Downloaded from https://onlinelibrary.wiley.com/doi/10.1002/hbm.26173 by South Korea National Provision, Wiley Online Library on [04/01/2024]. See the Terms and Conditions (https://onlinelibrary.wiley.com/terms-and-conditions) on Wiley Online Library for rules of use; OA articles are governed by the applicable Creative Commons License